TISSUE ENGINEERING: Part A Volume 00, Number 00, 2023 © Mary Ann Liebert, Inc. DOI: 10.1089/ten.tea.2023.0075



Open camera or QR reader and scan code to access this article and other resources online.



Cryopreservation Alters Tissue Structure and Improves Differentiation of Engineered Skeletal Muscle

Lauren Gapinske, PhD, 1,2 Lindsay Clark, PhD, 3,* Lourdes Marinna Caro-Rivera, BS, 2 and Rashid Bashir, PhD 1,2

Tissue-engineered skeletal muscle can play an important role in regenerative medicine, disease modeling, drug testing, as well as the actuation of biohybrid machines. As the applications of engineered muscle tissues expand, there exists a growing need to cryopreserve and store these tissues without impairing function. In a previous study, we developed a cryopreservation protocol in which engineered skeletal muscle tissues are frozen before myogenic differentiation. In that study, we found that this cryopreservation process led to a three-fold increase in the force generation of the differentiated muscle. Here, we perform further testing to determine the mechanisms by which cryopreservation enhances engineered skeletal muscle function. We found that cryopreservation alters the microstructure of the tissue by increasing pore size and decreasing elastic modulus of the extracellular matrix (ECM), which leads to increased expression of genes related to cell migration, cell-matrix adhesion, ECM secretion, and protease activity. Specifically, cryopreservation leads to the upregulation of many ECM proteins, including laminin, fibronectin, and several types of collagens, as well as integrins and matrix metalloproteinases. These changes to ECM structure and composition were associated with enhanced myogenic differentiation, as evidenced by the upregulation of late-stage myogenic markers and increased force generation. These results highlight the need to understand the effects of cryopreservation on the ECM of other tissues as we strive to advance tissue and organ cryopreservation protocols for regenerative medicine.

Keywords: tissue engineering, skeletal muscle, cryopreservation, extracellular matrix

Impact Statement

This study examines the effects of cryopreservation on engineered skeletal muscle tissue structure and uncovers the mechanisms by which these changes impact tissue development and function. These insights help inform the engineering of stronger muscle tissues and highlight the need to investigate cryopreservation-mediated changes to extracellular matrix as we develop suitable cryopreservation protocols for other tissues and organs.

Introduction

CRYOPRESERVATION REPRESENTS THE preferred method of long-term cell storage, as low temperatures suspend biological and chemical processes to prevent sample dete-

rioration. Although the process of freezing living cells typically results in cell death, the addition of cryoprotectants such as DMSO in combination with controlled freezing and thawing rates promotes cell survival by reducing ice crystal formation and osmotic stress. 1,2 While highly effective

¹Department of Bioengineering, University of Illinois at Urbana-Champaign, Urbana, Illinois, USA.

²Nick Holonyak Jr. Micro and Nanotechnology Laboratory, University of Illinois at Urbana-Champaign, Urbana, Illinois, USA.

³HPCBio, Roy J. Carver Biotechnology Center, University of Illinois at Urbana-Champaign, Urbana, Illinois, USA.

^{*}Current affiliation: Research Scientific Computing, Seattle Children's Research Institute, Seattle, Washington, USA.

methods to cryopreserve cell suspensions are commonly utilized, the cryopreservation of tissues has proven more difficult due to the variability in heat and mass transfer throughout the tissue.³ Thus, the cryopreservation of 3D tissues is typically associated with poor cell survival and significant damages to tissue structure and function.^{4–7}

The ability to overcome these limitations and successfully cryopreserve functional tissues is of great interest to the medical community, as it would enable the storage and shipment of tissues and organs used for medical treatments and scientific research. However, to improve current strategies for tissue cryopreservation, we also must understand the many effects of cryopreservation at the tissue level.

In this study, we use engineered skeletal muscle tissue as a model for the study of the effects of tissue cryopreservation. This work was motivated by the surprising results of a previous study, in which we discovered that cryopreservation of engineered C2C12 muscle ring constructs before myogenic differentiation led to an increase in force generation of the mature skeletal muscle tissue. SEM imaging seemed to reveal an apparent thinning of the extracellular matrix (ECM) coating on the surface of these 3D muscle rings in response to cryopreservation. However, this coating appeared to recover as the myoblasts differentiated. These results prompted us to further examine the effects of cryopreservation on skeletal muscle ECM structure and the mechanism by which these changes may enhance myogenic differentiation and force generation.

The ECM is known to play an essential role in controlling cell fate and establishing tissue structure and function. At a most basic level, the ECM serves as a scaffold, providing mechanical support for the growth and development of cells and tissues. In the ECM also interacts with specific cell receptors, enabling those cells to change their behavior in response to both the structure and composition of the surrounding ECM, as well as the growth factors it sequesters. Through these interactions, the ECM can affect cell proliferation, polarization, migration, differentiation, survival, and even apoptosis. Thus, it is to no surprise that any change to the ECM microstructure caused by the process of cryopreservation would alter the development of engineered skeletal muscle tissues.

In this study, we seek to further understand the mechanism by which cryopreservation leads to the enhanced differentiation of engineered skeletal muscle tissues. We investigate the impact of cryopreservation on the structure and stiffness of the ECM of engineered muscle tissues as they differentiate. We then use RNA-seq to measure gene expression and determine how these freezing-induced changes to the ECM impact myogenic differentiation at the molecular level.

Materials and Methods

Seeding of C2C12 myoblast rings

C2C12 murine myoblasts were cultured in growth medium (GM) consisting of Dulbecco's modified Eagle's medium with L-glutamine and sodium pyruvate (DMEM; Corning) supplemented with 10% v/v fetal bovine serum (FBS; Lonza), 1% v/v L-glutamine (Cellgro Mediatech), and 1% v/v penicillin-streptomycin (Cellgro Mediatech). Upon reaching $\sim 85\%$ confluency, cells were trypsinized and resuspended at a concentration of 1E7 cells mL⁻¹ within a matrix mixture of 30% v/v Matrigel (BD Biosciences),

4 mg mL $^{-1}$ fibrinogen (Sigma-Aldrich), and 0.5 U mg-fibrinogen $^{-1}$ thrombin (Sigma-Aldrich) in GM supplemented with 1 mg mL $^{-1}$ aminocaproic acid (ACA; Sigma-Aldrich) (GM+). The cell-matrix suspension (120 μ L) was pipetted into a PDMS injection ring mold and incubated at 37°C for 1 h before being immersed in GM+.

Three dimensional printing of PEGDA pillars

The pillar structures used to quantify skeletal muscle force generation were 3D printed using the Pico 2 (Asiga). The pillars were fabricated using 20% v/v polyethylene (glycol) diacrylate (PEGDA), 0.1% w/v lithium phenyl-2,4,6-trimethylbenzoylphosphinate (LAP; Sigma-Aldrich), and 0.04% w/v sunset yellow (Sigma-Aldrich). After fabrication, pillars were sterilized in 70% ethanol for 1 h, followed by overnight storage in phosphate-buffered saline (PBS).

Differentiation of myoblast rings

C2C12 myoblast rings were cultured for 3 days post-seeding in GM+ (refreshed daily). After 3 days, the myoblast rings were lifted from their molds and transferred to 3D pillars, where they were immersed in differentiation medium consisting of DMEM supplemented with 10% v/v heat inactivated horse serum (HS; Lonza), 1% v/v L-glutamine, and 1% v/v penicillin-streptomycin. Differentiation medium (DM) was further supplemented with 1 mg mL⁻¹ ACA and 50 ng mL⁻¹ human insulin-like growth factor-1 (IGF-1, Sigma Aldrich) (DM++). DM++ was refreshed daily for 7 days after ring transfer (Fig. 1a).

Freezing and thawing of undifferentiated myoblast rings

Twenty-four hours postseeding, undifferentiated C2C12 myoblast rings were removed from their molds and placed into cryogenic freezing tubes containing 1 mL warm GM supplemented with 5%, 10%, or 15% v/v dimethyl sulfoxide (DMSO; Fisher). Freezing tubes were placed in alcohol-free freezing containers (CoolCell; Corning) and stored in the -80°C freezer, where they were slowly frozen at a rate of 1°C min⁻¹. After 24h in the freezer, the cryogenic freezing tubes were placed in a warm 37°C water bath for ~3 min until completely thawed. The rings were then removed from the tubes, rinsed in PBS, and returned to their original ring molds to incubate for 48 h at 37°C. GM+ was refreshed daily. On day 4 postseeding, myoblast rings were transferred to 3D printed pillars and differentiated for 7 days in DM++ (Fig. 1b).

Force analysis

Upon the initiation of myogenic differentiation (day 3), muscle rings were transferred from ring molds to 3D printed PEGDA pillars (Fig. 1c, d). The muscle rings were placed in a dish with warm, serum-free DMEM. Two platinum electrodes were aligned parallel to the biobot to stimulate the muscle with 20 V, 50 ms pulses at 1 Hz. Videos of muscle contraction were used to calculate force through motion tracking with the video analysis software, Tracker (https://physlets.org/tracker). The distance between the two pillars was tracked over the course of 100 frames (~15 s depending on frame rate) to determine the force, calculated by the equation below. E represents the elastic modulus of the

pillars (269 kPa), I is the moment of inertia of the pillars, δ is the deflection of the pillars, a is the distance from surface to muscle, and L is the pillar height.

$$F = \frac{6EI\delta}{a^2(3L - a)}$$

Porosity measurement

To assess tissue porosity, samples were fixed, embedded in OCT solution, and sliced at a thickness of $20\,\mu m$ using the cryostat. Slices were imaged using a bright field microscope. Porosity was measured using ImageJ thresholded images. Pore size was calculated using the average feret diameter of the pores, and porosity was calculated using the percentage of total area covered by pores.

Elastic modulus measurement

The Piuma Nanoindenter (Optics11 Life) was used to measure the elastic modulus of live engineered skeletal muscle samples within contact solution liquid. Skeletal muscle rings were cut, laid flat, and held in place on the surface of the dish beneath a metal guard and magnets (Fig. 4a). The probe used to indent samples had a stiffness of 0.47 N/m with a tip radius of 51.5 μm . An approach and retraction speed of 2000 nm/s was used to indent the sample up to 2000 nm (Fig. 4b). To measure effective elastic modulus from the load indentation curve, a single fit Hertzian contact model with a Pmax of 80% was used, with a minimum R value of 0.95. Undifferentiated samples were analyzed $\sim 2 \, h$ after being thawed, or on day 1 in the case of the unfrozen samples. Differentiated samples were analyzed after 7 days of differentiation.

Cell density measurement

Engineered muscle tissues were fixed and cryosectioned to a thickness of 20 µm after 7 days of differentiation. Samples were permeabilized, blocked, and stained for DAPI (1:5000). Images were collected using the Zeiss Axioscan. Relative cell density between frozen and unfrozen samples was compared by measuring the percentage of fluorescent area using ImageJ.

MTS cell viability assay

Frozen and unfrozen muscle rings were collected after 7 days of differentiation. MTS solution (CellTiter 96 AQueous One Solution Cell Proliferation Assay; Promega) was thawed in a 37°C water bath and combined with warm DMEM (without phenol red) in a 1:5 volume ratio to form a working reagent. Muscle rings were rinsed in PBS, placed in individual wells of a 24-well plate, and immersed in MTS working reagent. The reaction was allowed to proceed in the dark for 4 h at 37°C. A microplate reader (Synergy HT; BioTek) was used to measure absorbance at 490 nm, which was then used to calculate relative viability between control and experimental samples.

RNA-seq gene expression analysis

Frozen and unfrozen muscle rings were analyzed both before and after differentiation. Frozen rings were collected 24 h after thawing (day 3) as well as after 7 days of differentiation (day 11). Unfrozen muscle rings were collected 24 h earlier for both time points (days 2 and 10). All muscle rings were snap frozen and stored at -80° C. Upon thawing, rings were homogenized by vortexing in RLT buffer (Qiagen) with $10\,\mu\text{L}$ mL⁻¹ B-mercaptoethanol and centrifuged using the QIAshredder (Qiagen) column. RNA was extracted using the RNeasy Plus RNA isolation kit (Qiagen) according to manufacturer's instructions.

RNAseq libraries were prepared with Kapa Hyper Stranded mRNA library kit (Roche). The libraries were pooled; quantitated by qPCR and sequenced on one SP lane for 101 cycles from one end of the fragments on a NovaSeq 6000. Fastq files were generated and demultiplexed with with the bcl2fastq v2.20 Conversion Software (Illumina). Average per-base read quality scores were over 30 in all samples and no adapter sequences were found, indicating that trimming was unnecessary.

The Mus musculus transcriptome file "GCF 000001635.27 GRCm39 rna.fna.gz" from Annotation 109 from NCBI was used for quasi-mapping and count generation. Salmon version 1.5.2 was used to quasi-map reads to the transcriptome and quantify the abundance of each transcript. The transcriptome was first indexed using the decoyaware method in Salmon with the entire genome file "GCF_000001635.27_GRCm39_genomic.fna.gz" as the decoy sequence. Then quasi-mapping was performed to map reads to transcriptome with additional arguments—seqBias and gcBias to correct sequence-specific and GC content biases, numBootstraps = 30 to compute bootstrap transcript abundance estimates and—validateMappings and—recoverOrphans to help improve the accuracy of mappings. Gene-level counts were then estimated based on transcript-level counts using the "lengthScaledTPM" method from the tximport package.

Percentage of reads mapped to the transcriptome ranged from 45.1% to 85.4% (Supplementary Fig. S1). The unmapped reads based on Salmon were discarded and the number of remaining reads (range: 15–51.2 million per sample) were kept for further analysis (Supplementary Fig. S2). STAR and featureCounts showed that samples with a lower percentage of reads mapping to the transcriptome tended especially to have more reads not mapping within a gene, and to a lesser extent more reads multimapped or unmapped (Supplementary Fig. S3). 13,14

When comparing expression levels, the numbers of reads per gene need to be normalized not only because of the differences in total number of reads, but because there could be differences in RNA composition such that the total number of reads would not be expected to be the same. The TMM (trimmed mean of M values) normalization in the edgeR package uses the assumption that most genes do not change to calculate a normalization factor for each sample to adjust for such biases in RNA composition (Supplementary Fig. S4). 15,16 While the NCBI GRCm39 Annotation 109 gene models have a total of 39,253 genes, many of these might not have detectable expression in these samples. Therefore, we set the detection threshold at 0.5 cpm (counts per million) in at least three samples, which resulted in 23,875 genes being filtered out, leaving 15,378 genes to be analyzed for differential expression that contain 99.95% of the reads.

After filtering, TMM normalization was performed again and normalized log2-based count per million values

(logCPM) were calculated using edgeR's cpm() function with prior.count=2 to help stabilize fold changes of extremely low-expression genes.¹⁷

Multidimensional scaling in the limma package was used as a sample QC step to check for outliers or batch effects (Supplementary Figs. S5 and S6). Differential gene expression (DE) analysis was performed using the limma-trend method. Gene expression was regressed against experimental group (treatment by timepoint), and the following contrasts were examined:

- Unfrozen_dif Unfrozen_undif: Normal differentiation of skeletal muscle rings
- Frozen_undif Unfrozen_undif: Difference between frozen and unfrozen myoblast rings before differentiation
- Frozen_dif Frozen_undif: Differentiation of muscle rings after freezing
- Frozen_dif Unfrozen_dif: Difference between frozen and unfrozen muscle rings after differentiation
- (Frozen_dif Frozen_undif) (Unfrozen_dif Unfrozen_undif): How differentiation progresses differently in cells that were frozen versus not

The limma package estimates a *p*-value and FDR-adjusted *p*-value for each gene and each contrast.²⁰ In addition, because multiple contrasts were examined, we calculated a "global" FDR-adjusted *p*-value for each gene and contrast, based on the distribution of *p*-values across all four contrasts; this increased the number of significant hits for the interaction and for comparisons of frozen to unfrozen muscle rings, and decreased the number of significant hits for comparisons of the two time-

points. Table 3.1 shows the number of significantly up- and downregulated genes for each contrast at global FDR <0.05. Gene set enrichment analysis was performed with the goana and kegga functions from the limma R package, with trend=TRUE to adjust for gene abundance and a local FDR cutoff of 0.05.

Statistical Analysis

In all bar graphs, data are represented as the mean \pm standard deviation. The Student's t test was used to determine significance, with $p < 0.05^*$, $p < 0.01^{**}$, $p < 0.001^{***}$. In box charts, data within the box represents the interquartile range (25th–75th percentile), with the center line representing the median and point representing the mean. The whiskers extend from the 5th–95th percentile.

Results

Cryopreservation leads to increased force production of engineered muscle

In a previous study, we used optogenetic C2C12 myoblasts (ChR2-C2C12) to form a 3D muscle ring surrounding a 3D printed locomotive "biobot" structure. This engineered skeletal muscle "biobot" served as a model to optimize a protocol for the cryopreservation of engineered skeletal muscle tissue. We cryopreserved muscle rings at two time points: before and after myogenic differentiation and compared outcomes. Upon maturation, we found that those engineered muscle tissues which had previously been frozen while undifferentiated generated forces three-fold higher than the unfrozen control, while muscle tissues which

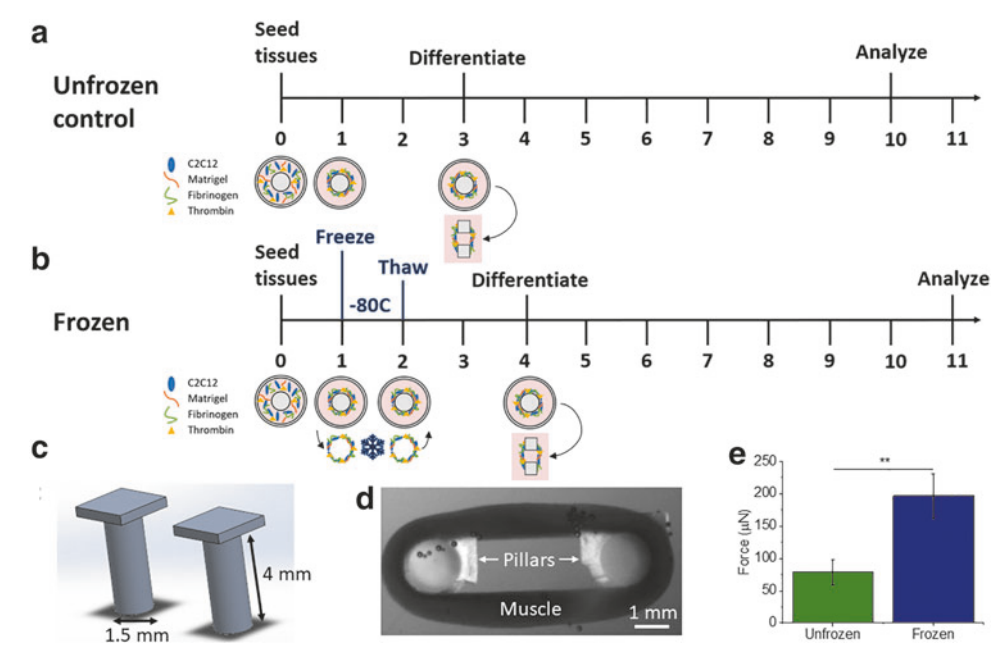


FIG. 1. Timeline for skeletal muscle ring fabrication for unfrozen control (a) and cryopreserved muscle rings (b). Skeletal muscle rings are seeded on day 0 using a previously published protocol [21]. Rings are frozen on day 1 for a period of 24 h, then returned to culture after a rapid thaw. Unfrozen control myoblast rings are transferred to pillar structures and switched to differentiation medium on day 3, and eventually analyzed on day 10, when differentiation is complete. The timeline for frozen muscle differentiation is shifted by 1 day due to the "null time" while frozen. This protocol is consistent with that previously published. (c) CAD design of 3D printed pillars used to quantify skeletal muscle ring force production. (d) *Top*view image of skeletal muscle ring wrapped around 3D printed PEGDA pillars. (e) Force generation of muscle calculated through quantification of pillar deflection under electrical stimulation of muscle (N=4, **p<0.01, standard deviation).

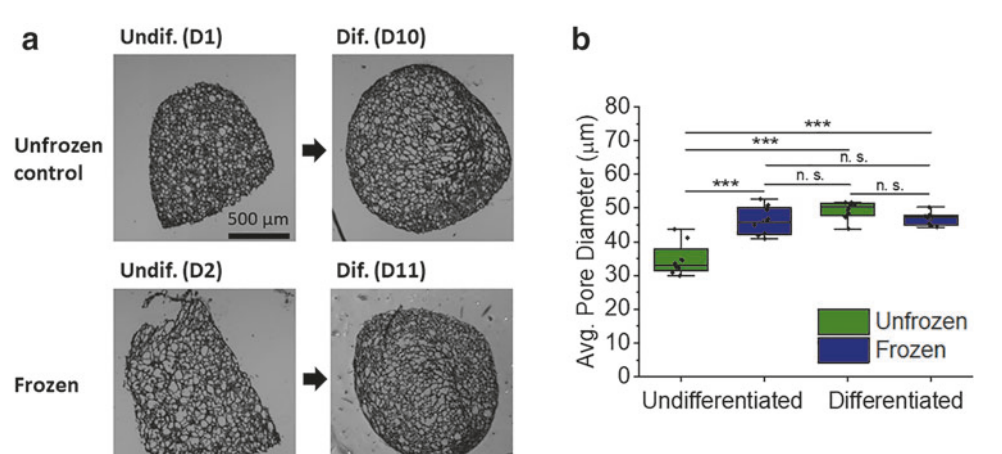


FIG. 2. Porosity of frozen versus unfrozen muscle rings both before and after differentiation. (a) $10 \, \mu m$ cross-sectional slices were imaged using a bright field microscope to assess tissue porosity. (b) Pore size was determined by measuring the average feret diameter of pores (N=8, ***p<0.001, n.s.=not significant).

had been frozen after undergoing myogenic differentiation showed significantly impaired force generation. Based on these results, we developed an optimized protocol (Fig. 1), in which myoblast rings are frozen in growth media containing 10% DMSO 24h after tissue seeding. The next day, rings are thawed and returned to cell culture, where they are allowed to recover and are eventually induced to differentiate into mature muscle.

In this current work, we chose to study only these engineered muscle tissues which were frozen while undifferentiated, as cryopreservation at this time point led to enhanced force generation of the mature muscle. We sought to replicate the results of our previous study by forming muscle rings with wild-type C2C12 myoblast cells and using fixed pillars adhered to a glass slide to track tissue force generation, as opposed to the locomotive biobot structure (Fig. 1). Consistent with prior results, we observed significant 2.5-fold increase in force generation of the frozen tissues (196 \pm 34 μN) vs the unfrozen control (79 \pm 20 μN) (Fig. 1e). These results demonstrate a consistent positive effect of cryopreservation on engineered skeletal muscle development and function.

Cryopreservation increases ECM pore size

In our prior work, SEM imaging suggested a change in ECM thickness in response to the cryopreservation of myoblast rings. ECM microstructure is known to play an important role in cell growth and differentiation. Thus, to elucidate the mechanism by which cryopreservation leads to enhanced force generation of skeletal muscle, we began by assessing the effects of cryopreservation on ECM microstructure. We sought to uncover how the freeze-thaw process alters ECM microstructure, as well as how the tissue microstructure changes throughout differentiation. We compared images of cross-sectional slices of frozen and unfrozen muscle rings both immediately after freezing as well as after the tissues had differentiated (Fig. 2a). Frozen, undifferentiated myoblast rings had a significantly larger average pore size than the unfrozen, undifferentiated control $(46\pm4\,\mu\text{m}$ and $35\pm5\,\mu m$ Feret diameter, respectively) (Fig. 2b).

After differentiation, however, the difference in pore size between frozen and unfrozen tissues was not significant $(47\pm2\,\mu m$ and $49\pm3\,\mu m$, respectively) (Fig. 2b). These results show that cryopreservation causes an immediate in-

crease in ECM pore size, which does not significantly change as the frozen myoblast ring differentiates. Unfrozen control myoblast rings, however, do exhibit an increase in pore size (35 μ m to 49 μ m) as they differentiate. Interestingly, the increase in pore size caused by cryopreservation is similar to that which naturally occurs throughout differentiation of the unfrozen tissue, resulting in similar pore sizes between the frozen and unfrozen tissues by the time they fully differentiate (Fig. 2b).

Cryopreservation does not affect cell density of differentiated muscle rings

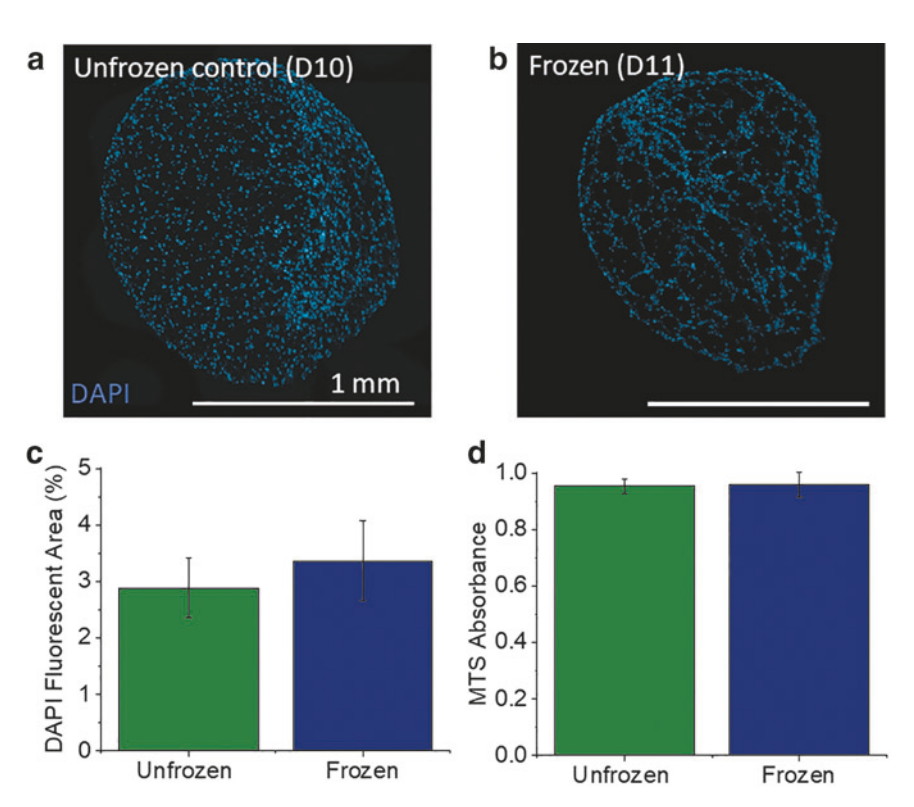
To elucidate the mechanism by which cryopreservation and the resulting changes to ECM microstructure leads to enhanced force generation of differentiated muscle, we began by assessing the effect of cryopreservation on cell number. We believed that the increase in ECM porosity could potentially lead to enhanced nutrient and waste perfusion throughout the 3D construct, resulting in better cell survival or proliferation. An increase in cell number, as a result of cryopreservation, could explain the increase in force generation. To assess cell number, we imaged differentiated muscle cross-sections stained with DAPI to label cell nuclei and compared the percent area of the fluorescent DAPI signal (Fig. 3a, b). These images showed no apparent difference in cell number throughout the cross-sectional area of frozen and unfrozen tissues $(3.4\pm0.7\,\mu\text{m})$ and $2.9\pm0.5\,\mu\text{m}$ (Fig. 3c).

In addition to measuring the DAPI signal, we used an MTS assay to measure the metabolic activity of cells within frozen and unfrozen differentiated tissues. This signal can be used to compare the relative cell viability between groups. Again, we observed no significant difference in the number of viable cells between frozen and unfrozen differentiated tissues $(0.96\pm0.04~\text{AU}$ and $0.95\pm0.03~\text{AU}$ absorbance at 490~nm) (Fig. 3d). These results indicate that the resulting increase in force generation of frozen tissues is not caused by an increase in cell density.

Cryopreservation causes decrease in elastic modulus of myoblast rings

The microstructure of a given material is closely related to its mechanical properties. The elastic modulus of fibrin, a major component of our skeletal muscle rings, for instance,

FIG. 3. Quantification of cell number in frozen versus unfrozen skeletal muscle rings. Images of tissue cross sections were taken for both unfrozen (a) and frozen (b) differentiated muscle tissue samples. (c) DAPI fluorescent area is compared between frozen and unfrozen muscle as a means to compare cell density in tissue cross sections. (N=9, p=0.12, standard deviation) (d) An MTS cell viability assay was performed to quantify the relative cell number in unfrozen and frozen live muscle rings (N=3,p = 0.84, standard deviation). No significant difference was observed between groups.



has been shown to increase as the pore size of the matrix is decreased. Hurthermore, the elastic modulus of various substrate materials has been consistently shown to impact the differentiation of many cell types, including skeletal muscle. We used the Piuma nanoindenter to measure the elastic modulus of frozen and unfrozen muscle rings both before and after differentiation, to evaluate how cryopreservation impacts elastic modulus (Fig. 4). Cryopreservation led to a significant decrease in elastic modulus of frozen myoblast rings compared to the unfrozen, undifferentiated control $(0.55 \pm 0.12 \,\mathrm{kPa})$ and $2.44 \pm 1.83 \,\mathrm{kPa}$, respectively) (Fig. 4d).

By the time these rings had differentiated, however, the difference in elastic modulus between frozen and unfrozen tissues was insignificant $(1.37\pm0.96\,\mathrm{kPa}$ and $1.77\pm0.27\,\mathrm{kPa})$. When we look at the change in elastic modulus as muscle rings differentiate, we see no significant change in the elastic modulus of unfrozen rings, despite an increase in ECM pore size. In the case of frozen muscle rings, however, we observe a significant increase in elastic modulus, despite no change in ECM pore size as the myoblasts differentiate (Fig. 4d). From these results, we conclude that the process of cryopreservation not only impacts ECM pore size, but also elastic modulus of the engineered muscle ring.

Relationship between pore size and elastic modulus of the muscle ring

When we examine together the changes in pore size of the ECM and elastic modulus of the muscle ring throughout differentiation, we see that relative increases in pore size of the ECM are generally associated with decreases in elastic modulus (Fig. 4e). In the case of the unfrozen muscle, as

differentiation occurs, elastic modulus decreases while ECM pore size increases (Supplementary Fig. S7a). As a result of cryopreservation, we initially observe a relative decrease in elastic modulus and increase in ECM pore size compared to the unfrozen, undifferentiated control (Supplementary Fig. S7b). However, as differentiation occurs, elastic modulus increases, despite pore size remaining constant (Fig. 4e). This seems to suggest that changes to the composition of the ECM itself, as opposed to the porosity, are driving the increase in elastic modulus throughout differentiation.

Cryopreservation alters RNA expression throughout differentiation

To better understand the molecular mechanisms at play during the response to cryopreservation, RNA expression of frozen and unfrozen skeletal muscle rings was compared both before and after differentiation. Frozen, undifferentiated myoblast rings were allowed to recover for 24 h in culture upon thawing before samples were collected for RNA-seq analysis. Differentiated muscle rings were collected once the muscle had differentiated for 7 days. Samples were compared using five contrasts, as indicated in Figure 5b. An F-test was performed to identify genes with significant variance in expression, and a total of 10,244 genes were found to be significant at FDR <0.05. A heatmap of these genes is shown in Figure 5a.

An interaction test comparing the change in gene expression of frozen vs unfrozen muscle rings as they differentiated indicated a significant downregulation of 604 genes, and a significant upregulation of 962 genes, with 13,812 genes being unaffected (Fig. 5b). This indicates that the freezing process alters the relative change in gene expression throughout myogenic differentiation. Gene set

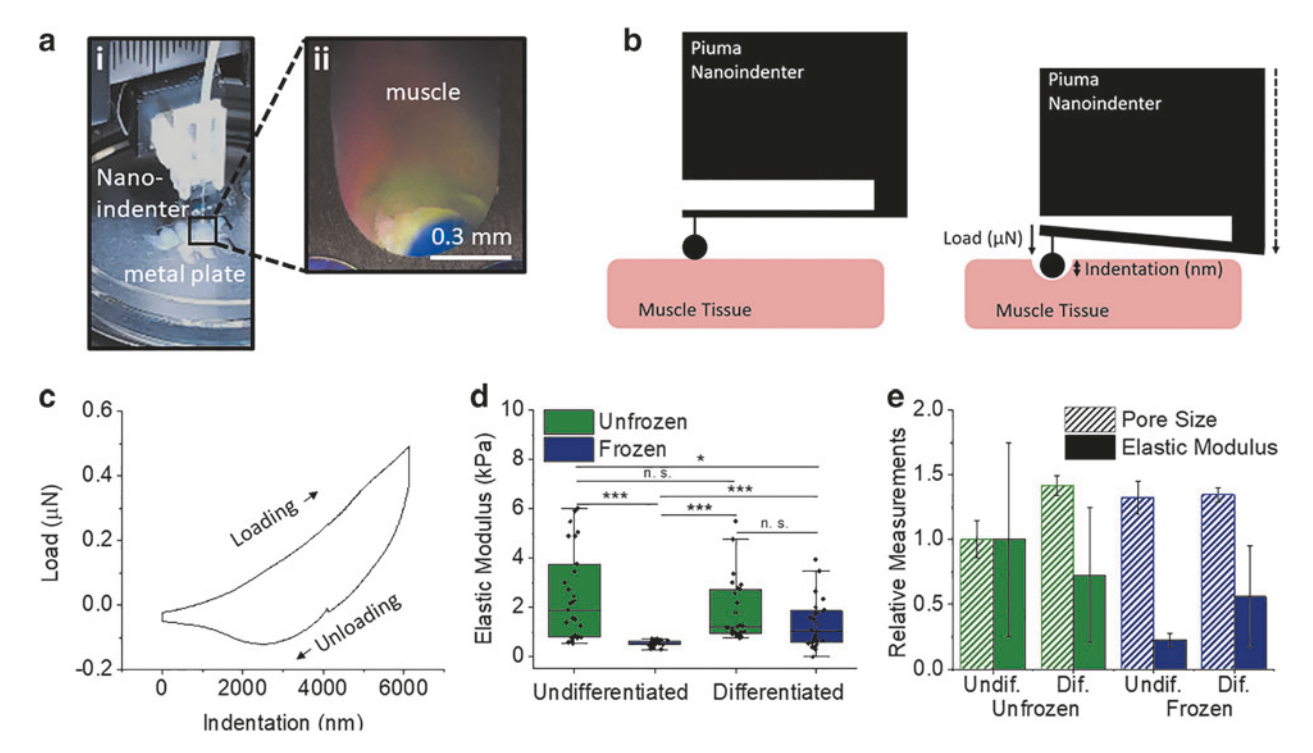


FIG. 4. Elastic modulus measurements of muscle rings. (a) Piuma Nanoindenter setup used to quantify elastic modulus of muscle rings. (i) Image showing placement of dish filled with contact solution beneath indentation probe. Skeletal muscle ring fixed to the *bottom* of the dish using a metal grid held by a magnet. (b) Schematic showing Piuma nanoindenter positioning on muscle ring pre- and postloading. When the spherical probe touches the tissue, the cantilever bends and displacement are detected by an optical fiber. (ii) Close-up image showing muscle ring exposed through metal grid. (c) Example of load indentation curve used to quantify effective elastic modulus. *Top* curve represents loading, while *bottom* curve represents unloading of the probe on the sample. (d) Effective elastic modulus of frozen and unfrozen tissues while undifferentiated and differentiated (N=27, ****p<0.001, *p<0.05, n.s.=not significant). (e) Pore size and elastic modulus of unfrozen samples relative to unfrozen undifferentiated samples (Pore Size N=8, Elastic Modulus N=27).

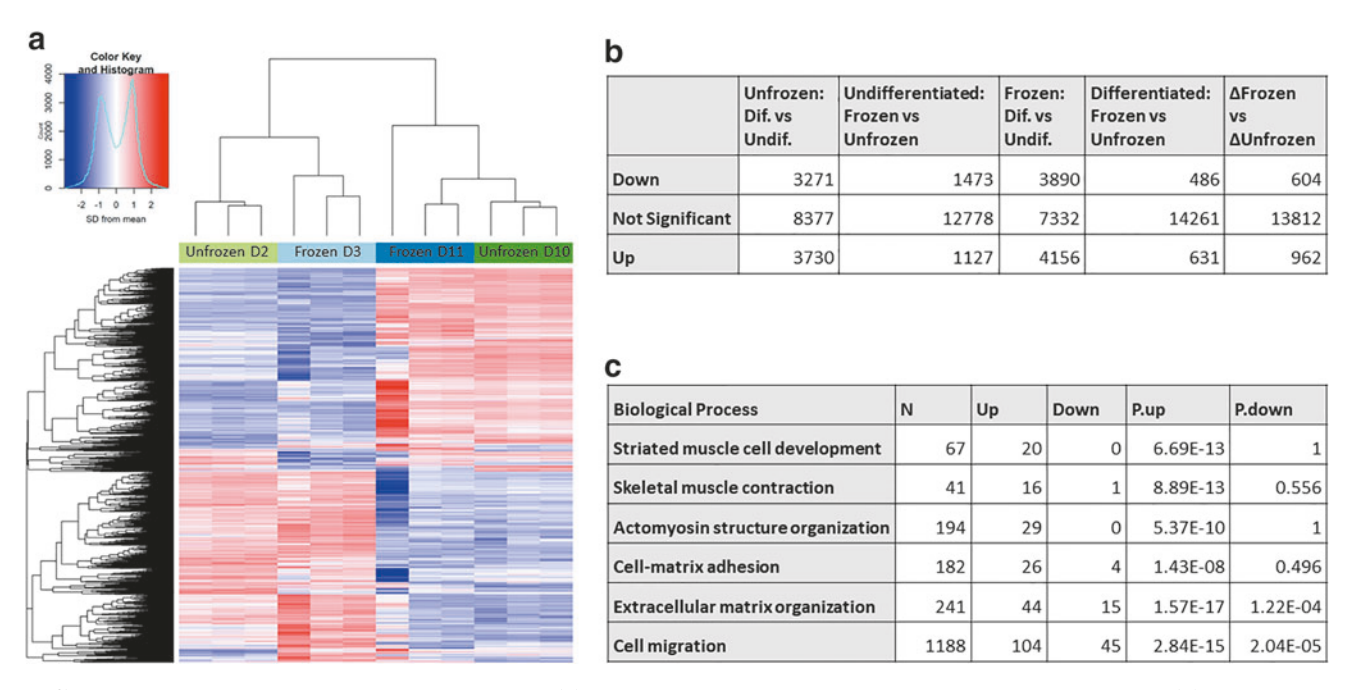


FIG. 5. RNA-seq analysis of gene expression. (a) Heatmap of 10,244 significant genes from ANOVA. (b) Number of genes significantly up- and downregulated in each contrast at global FDR <0.05. (c) Gene ontology results for biological processes significantly altered in frozen samples throughout differentiation compared to unfrozen samples, (Frozen dif.–Frozen undif.) – (Unfrozen dif.–Unfrozen undif.).

enrichment analysis was performed to determine the gene ontology biological process to which the significantly regulated genes belonged. Selected processes with p < 1e-5 were compiled in Figure 5c, each of which showed a significant change in the expression of genes in these pathways throughout the differentiation of frozen muscle rings, compared to unfrozen rings. As would be expected based on force data, we see a significant upregulation of genes related to striated muscle cell development, skeletal muscle contraction, and actomyosin structure organization.

We also see significant upregulation of genes in processes related to ECM organization and cell-matrix adhesion, which is unsurprising given the observed changes to the ECM microstructure and mechanical properties of frozen muscle rings throughout differentiation, compared to the unfrozen control. Finally, we also notice significant changes in genes related to cell migration, indicating enhanced cell motility in the frozen vs unfrozen muscle rings as they differentiate.

We next compared the expression of specific genes in frozen vs. unfrozen differentiated muscle rings. Selected genes are categorically reported in Figure 6a and plotted in Figure 6b. ECM proteins upregulated in differentiated frozen muscle rings compared to the unfrozen control include fibronectin, laminin, collagen (I, IV, XI, XV, XIV, VIII), dermatopontin, and fibromodulin. Collagen XII, however, is downregulated in frozen muscle. Integrins alpha 8, alpha 1, and beta-like 1 are upregulated in frozen muscle rings. Proteases cathepsin C, matrix metallopeptidases (MMPs) 8 and 10 are also upregulated, while *MMP 13* is downregulated.

These results suggest that frozen muscle rings not only secrete but organize and interact with ECM in an altered manner in response to cryopreservation. RNA seq analysis also showed increased expression of many late-stage myogenic markers, including myogenic factor 6, tropomyosin and myosin proteins, as well as insulin-like growth factor 1, indicating relative tissue maturity as well as superior force generation capability. Likewise, myogenic factor 5, an early-stage myogenic marker, is downregulated in frozen muscle rings, indicating a lower abundance of undifferentiated myoblasts.

The results of this study allowed us to develop a proposed mechanism by which cryopreservation leads to increased force generation of engineered muscle tissues (Fig. 7). We hypothesize that extracellular ice crystals form during the cryopreservation process, and the formation of these ice crystals leads to the observed increase in ECM pore size. This increased pore size is associated with a temporary decrease in the measured elastic modulus of the muscle ring, and appears to stimulate significant increases in ECM, integrin, and protease expression, as observed by RNA-seq analysis. Variation in the expression levels of specific ECM proteins, integrins, and proteases work synergistically to drive further changes in the expression levels and activity of these proteins.

ECM expression increases the elastic modulus of the muscle ring, resulting in mechanical signaling that can enhance differentiation. ECM expression in combination with integrin sensing results in chemical signaling that can also direct muscle differentiation. Furthermore, integrin sensing of the ECM in combination with protease degradation of the

a				Log Fold Change	Global FDR
	ECM	Fndc1	fibronectin type III domain containing 1	1.805	4.56E-05
		Lama3	laminin, alpha 3	2.347	6.31E-05
		Col4a5	collagen, type IV, alpha 5	0.8588	0.009972
		Col12a1	collagen, type XII, alpha 1	-1.112	9.33E-05
		Col1a1	collagen, type I, alpha 1	1.414	0.000446
		Col11a1	collagen, type XI, alpha 1	1.218	0.001162
		Col15a1	collagen, type XV, alpha 1	1.174	0.001416
		Col8a2	collagen, type VIII, alpha 2	2.364	0.001692
		Col8a1	collagen, type VIII, alpha 1	1.779	3.93E-05
		Col14a1	collagen, type XIV, alpha 1	2.751	6.54E-08
		Dpt	dermatopontin	2.101	7.87E-06
		Fmod	fibromodulin	4.154	2.21E-05
	Integrin	Itga8	integrin alpha 8	1.541	0.005203
		ltga1	integrin alpha 1	1.165	0.006302
		ltgbl1	integrin, beta-like 1	2.045	0.000204
	Protease	Ctsc	cathepsin C	1.669	0.000447
		Mmp8	matrix metallopeptidase 8	3.448	0.004044
		Mmp10	matrix metallopeptidase 10	1.99	0.004134
		Mmp13	matrix metallopeptidase 13	-1.382	4.48E-05
	Myogenie Marker	Tpm1	tropomyosin 1, alpha	0.8468	0.003017
		Tpm3	tropomyosin 3, gamma	0.8377	0.002035
		Mylk3	myosin light chain kinase 3	1.164	0.005456
		Mybpc1	myosin binding protein C, slow-type	1.125	0.01941
			myosin, heavy polypeptide 4, skeletal		
		Myh4	muscle	0.9815	0.02359
		Myh8	myosin, heavy polypeptide 8, skeletal muscle, perinatal	0.4758	0.05124
			myosin, heavy polypeptide 1, skeletal		
		Myh1	muscle, adult	0.5374	0.06355
		Myf6	myogenic factor 6	1.331	0.0165
		Myf5	myogenic factor 5	-0.945	0.001431
		lgf1	insulin-like growth factor 1	2.049	0.000243

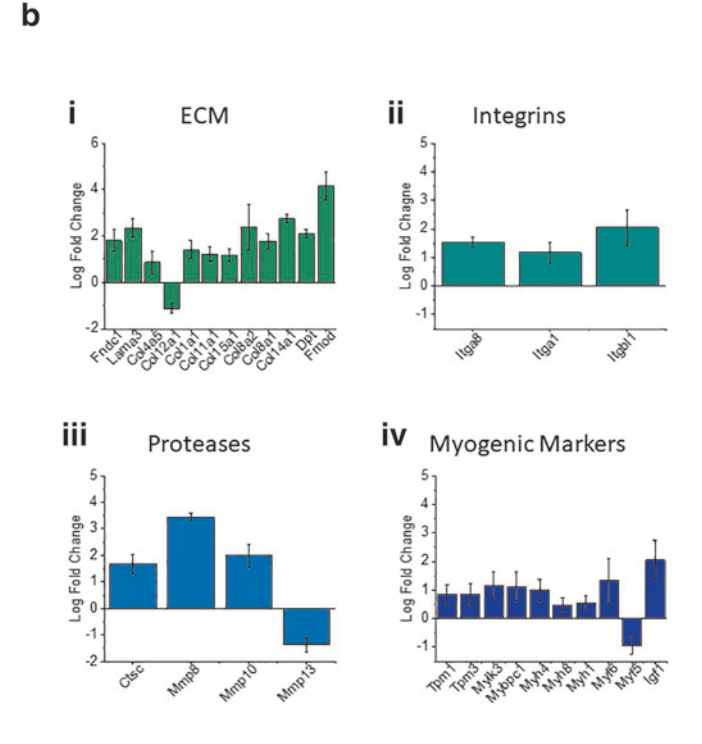


FIG. 6. (a) Genes with significantly altered expression levels in frozen differentiated samples compared to unfrozen differentiated samples. (b) Plots of differentially expressed genes listed in part a. (i) ECM components, (ii) Integrins, (iii) Proteases, and (iv) Myogenic markers (N=3, standard deviation). ECM, extracellular matrix.

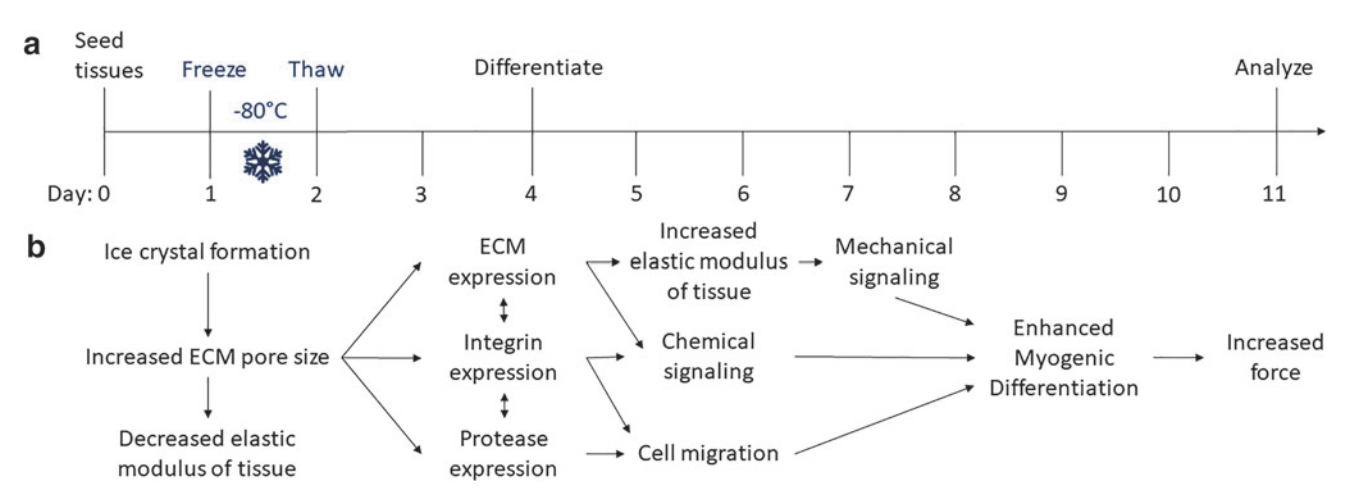


FIG. 7. (a) Timeline of engineered skeletal muscle tissue seeding, cryopreservation, and differentiation. (b) Schematic outlining the proposed model by which cryopreservation leads to enhanced function when engineered muscle tissues are frozen before differentiation.

ECM can enable cell migration, which is essential for myoblast fusion, a critical step in muscle differentiation. Finally, this enhanced differentiation of myoblasts into more mature myotubes with increased expression of proteins involved in muscle contraction leads to an overall increase in the force of the engineered muscle tissue (Fig. 7). The results of this work are summarized in Figure 7, which outlines the proposed mechanism by which cryopreservation leads to a gain of function in engineered muscle tissues.

Discussion

Ice crystal formation is a major contributor to cell death during the cryopreservation process. Intracellular ice crystal formation is thought to be particularly lethal, as it can lead to mechanical damage to organelles and the cell membrane. To prevent intracellular ice crystal formation, many cryopreservation methods involve a relatively slow freezing rate, which allows water to flow out of the cells before the crystallization process. Cell-permeating cryoprotectants such as DMSO reduce ice crystal formation by lowering the freezing point and disrupting ice crystal growth both inside and outside the cell. However, due to the cytotoxicity of cryoprotectants such as DMSO, their concentration must be limited, and there exists a balance between acceptable ice crystal formation and cryoprotectant concentration.

Extracellular ice crystal formation has been shown to increase the pore size of 3D scaffolds such as gelatin during cryopreservation, with a correlation to DMSO cryoprotectant concentration. Although DMSO can reduce the size of ice crystals that form, at nonlethal concentrations and slow cooling rates, DMSO cannot entirely prevent ice crystal formation. In this study, we examined the impact of extracellular ice crystal formation on pore size by imaging frozen and control muscle ring cross sections both before and after myogenic differentiation. As would be expected, cryopreservation led to a significant increase in ECM pore size.

Pore size has long been considered an important parameter for the engineering of 3D cell scaffolds. Sufficient ECM pore size is essential for cell growth, migration, and nutrient flow. However, smaller pore sizes correspond to higher ECM surface area, which is essential for cell adhesion and

the cell-ECM signaling that guides proliferation, migration, and differentiation.²⁷ We recognized that this increase in ECM pore size could potentially impact myoblast health and behavior in myriad ways, leading to the enhanced functionality we observe in frozen muscle rings. We first examined the viability of cells throughout the differentiated muscle ring, as enlarged pore size could potentially increase nutrient perfusion and waste removal, leading to greater proliferation and cell survival.²⁸

An increase in myotube density throughout the muscle ring would likely lead to an increase in overall force generation. However, MTS viability assays as well as cell counting proved that the observed increase in force generation of frozen muscle rings could not be explained by an increase in cell number. These results indicated that the force production of individual myotubes must have increased as a result of the cryopreservation process.

The elastic modulus of a cell substrate is widely known to impact cell differentiation. Skeletal muscle myoblasts have been found to differentiate most optimally on substrates with tissue-like stiffness of $\sim 12\,\mathrm{kPa.}^{22}$ When we measured the compressive elastic modulus of frozen myoblast rings, however, we found that the cryopreservation process lowers elastic modulus to a level further from that of native muscle tissue. Furthermore, the stiffness of frozen rings is increased throughout differentiation such that it is no longer different from that of the unfrozen control, indicating that the enhanced performance of these frozen muscle rings most likely cannot be explained by an optimization of substrate stiffness.

Although elastic modulus is typically inversely correlated with pore size, we found that when frozen muscle rings differentiated, an increase in elastic modulus was observed independent of a change in pore size. This suggests that the composition of the ECM, rather than its microstructure, is likely changing as the engineered muscle matures.

The ECM interacts with cells to provide important information about the microenvironment through both biochemical and mechanical signaling. This signaling is essential in the control of cell behavior and development. Cells sense the ECM through surface receptors, and through this interaction, processes, including cell proliferation,

polarization, migration, differentiation, and apoptosis, are controlled. These processes are also impacted by the protease degradation of ECM, which releases ECM-bound growth factors and enables them to bind to cell surface receptors.

Changes in ECM pore size have been shown to cause changes in cell secretion of ECM proteins.²⁹ This stimulation of ECM secretion could provide more optimal chemical and mechanical signaling for myogenic differentiation, leading to enhanced skeletal muscle function. Through RNA seq analysis, we found that frozen muscle rings differentially expressed many ECM proteins, including dermatopontin, a protein known to promote myoblast differentiation in C2C12s, as well as fibromodulin, which is positively regulated with dermatopontin and suppresses myostatin, an inhibitor to muscle growth. 30 Laminin, a basal lamina protein known to promote the expression and activation of integrins as well as the proliferation, differentiation, and adhesion of muscle cells, is upregulated, in addition to fibronectin, which also promotes differentiation and facilitates the fusion and linear alignment of myotubes during differentiation.³

Finally, several subtypes of collagen, the most abundant ECM component of skeletal muscle, are differentially expressed as well. This includes upregulation of collagen type IV, which is one of the main components of the basal lamina and promotes IGF-1-mediated migration, differentiation, and fusion of myoblasts. 31 Collagen type I, which has been shown to promote C2C12 myoblast migration and differentiation, is also upregulated.³² Fibrillar collagens such as type 1 have also been shown to increase skeletal muscle stiffness, protecting smaller muscle fibers from damage.³¹ This increase in fibrillar concentration likely helps to explain the relative increase in elastic modulus of the frozen muscle ring throughout differentiation. In addition to the differential expression of ECM proteins, frozen muscle rings also express higher levels of integrins, which tether the cytoskeleton to ECM, enabling cells to sense their external microenvironment.

Integrins regulate the adhesion, proliferation, migration, and differentiation of myoblasts, as well as force transmission within the engineered muscle.³¹ Cryopreservation also increases expression of proteases, including cathepsin C and several MMPs, which aid in the degradation and remodeling of the ECM.³³ This is essential for myoblast migration and differentiation, as it serves to eliminate the intercalating ECM between myoblasts and allow cell fusion.³³ It is worth noting that native skeletal muscle tissue consists of additional cell types, including endothelial and fibro-adipogenic progenitor cells, which also contribute to ECM composition, and whose presence may impact changes in ECM secretion in response to cryopreservation. Unsurprisingly, RNA seg also revealed increased expression of key proteins for muscle force generation, including tropomyosin and myosin, as well as IGF-1, which stimulates muscle hypertrophy. 34-36

Conclusion

Cryopreservation of engineered skeletal muscle tissues before differentiation has been shown to facilitate an increase in force generation of the mature muscle. In this study, we found that cryopreservation increases the pore size of engineered muscle tissue and stimulates the expression of various ECM proteins, integrins, and proteases. Together, these changes to ECM structure and composition enhance myoblast migration and differentiation, leading to the upregulation of proteins essential for muscle contraction and a functional improvement in cryopreserved muscle. In the future, we can use the knowledge gained from this study to modify our approach to engineering skeletal muscle tissues to achieve larger pore size, as well as provide key ECM proteins shown to be associated with enhanced muscle differentiation and force production, to engineer stronger skeletal muscle tissues.

Furthermore, this study highlights a greater need to understand the effects of cryopreservation on the ECM of other tissue types, to develop tissue-specific cryopreservation protocols which best maintain tissue health and function.

Acknowledgments

The authors thank Dr. Jessica Spear from the Seitz Materials Research Laboratory for assistance with elastic modulus measurements, Dr. Alvaro Gonzalo Hernandez and Dr. Chris Wright from the Roy J. Carver Biotechnology Center for their assistance with library preparation and RNA sequencing, and Dr. Mayandi Sivaguru from the Microscopy and Imaging Core Facilities of the Carl R. Woese Institute for Genomic Biology for insight regarding sample preparation for ECM imaging. The authors also thank Dr. Gelson Pagan-Diaz for insightful discussion regarding proposed experimental techniques.

Authors' Contributions

L.G. designed and performed experiments, analyzed data, and prepared the article. L.C. analyzed RNA-seq data and edited the article. L.M.C.R. performed experiments. R.B. led the project, contributed to the design of experiments, and edited the article.

Disclosure Statement

No competing financial interests exist.

Funding Information

This work was funded by National Science Foundation (NSF) Science and Technology Center Emergent Behavior of Integrated Cellular Systems (EBICS) Grant CBET0939511. LG was funded by NSF Research Traineeship in Understanding the Brain (NRT-UtB): Training the Next Generation of Researchers in Engineering and Deciphering of Miniature Brain Machinery, Grant 1735252.

Supplementary Material

Supplementary Figure S1

Supplementary Figure S2

Supplementary Figure S3

Supplementary Figure S4

Supplementary Figure S5

Supplementary Figure S6

Supplementary Figure S7

References

- Jang TH, Park SC, Yang JH, et al. Cryopreservation and its clinical applications. Integr Med Res 2017;6(1):12; doi: 10 .1016/J.IMR.2016.12.001
- Bakhach J. The cryopreservation of composite tissues: Principles and recent advancement on cryopreservation of different type of tissues. Organogenesis 2009;5(3):119; doi: 10.4161/ORG.5.3.9583
- 3. Xu F, Moon S, Zhang X, et al. Multi-scale heat and mass transfer modelling of cell and tissue cryopreservation. Philos Trans R Soc A Math Phys Eng Sci 2010;368(1912): 561–583; doi: 10.1098/rsta.2009.0248
- 4. Alink GM, Verheul CC, Agterberg J, et al. Viability and Morphology of rat heart cells after freezing and thawing of the whole heart. Cryobiology 1978;15(1):44–58; doi: 10.1016/0011-2240(78)90006-8
- Gimeno MJ, Pascual G, Garcia-Honduvilla N, et al. Arterial damage induced by cryopreservation is irreversible following organ culture. Eur J Vasc Endovasc Surg 1999;17(2):136–143; doi: 10.1053/EJVS.1998.0739
- Rubinsky B, Pegg DE. A mathematical model for the freezing process in biological tissue. Proc R Soc London Ser B Biol Sci 1988;234(1276):343–358; doi: 10.1098/ RSPB.1988.0053
- Pegg DE. The relevance of ice crystal formation for the cryopreservation of tissues and organs. Cryobiology 2010; 60(3):S36–S44; doi: 10.1016/J.CRYOBIOL.2010.02.003
- Grant L, Raman R, Cvetkovic C, et al. Long-term cryopreservation and revival of tissue-engineered skeletal muscle. Tissue Eng Part A 2019;25(13–14):1023–1036; doi: 10.1089/ten.tea.2018.0202
- Pizzo AM, Kokini K, Vaughn LC, et al. Highlighted topic biomechanics and mechanotransduction in cells and tissues extracellular matrix (ECM) microstructural composition regulates local cell-ECM biomechanics and fundamental fibroblast behavior: A multidimensional perspective. J Appl Physiol 2005;98(5):1909–1921; doi: 10.1152/japplphysiol .01137.2004
- Frantz C, Stewart KM, Weaver VM. The extracellular matrix at a glance. J Cell Sci 2010;123(24):4195–4200; doi: 10.1242/JCS.023820
- Thorsteinsdottir S, Deries M, Cachaço AS, et al. The extracellular matrix dimension of skeletal muscle development. Dev Biol 2011;354(2):191–207; doi: 10.1016/J.YDBIO.2011.03.015
- 12. Ingber DE. Mechanical control of tissue morphogenesis during embryological development. Int J Dev Biol 2003;50(2–3):255–266; doi: 10.1387/IJDB.052044DI
- 13. Dobin A, Davis CA, Schlesinger F, et al. STAR: Ultrafast universal RNA-seq aligner. Bioinformatics 2013;29(1):15–21; doi: 10.1093/BIOINFORMATICS/BTS635
- Liao Y, Smyth GK, Shi W. Featurecounts: An efficient general purpose program for assigning sequence reads to genomic features. Bioinformatics 2014;30(7):923–930; doi: 10.1093/BIOINFORMATICS/BTT656
- Robinson MD, Oshlack A. A scaling normalization method for differential expression analysis of RNA-seq data. Genome Biol 2010;11(3):R25; doi: 10.1186/GB-2010-11-3-R25
- Robinson MD, McCarthy DJ, Smyth GK. edgeR: A Bioconductor package for differential expression analysis of digital gene expression data. Bioinformatics 2010;26(1): 139–140; doi: 10.1093/BIOINFORMATICS/BTP616

- 17. McCarthy DJ, Chen Y, Smyth GK. Differential expression analysis of multifactor RNA-Seq experiments with respect to biological variation. Nucleic Acids Res 2012;40(10): 4288; doi: 10.1093/NAR/GKS042
- Ritchie ME, Phipson B, Wu D, et al. limma powers differential expression analyses for RNA-sequencing and microarray studies. Nucleic Acids Res 2015;43(7):e47; doi: 10.1093/NAR/GKV007
- Chen Y, Lun ATL, Smyth GK. From reads to genes to pathways: Differential expression analysis of RNA-Seq experiments using Rsubread and the edgeR quasilikelihood pipeline. F1000Res 2016;5:1438; doi: 10.12688/ f1000research.8987.2
- Benjamini Y, Hochberg Y. Controlling the false discovery rate: A practical and powerful approach to multiple testing. J R Stat Soc Ser B 1995;57(1):289–300; doi: 10.1111/J .2517-6161.1995.TB02031.X
- 21. Mooney R, Tawil B, Mahoney M. Specific fibrinogen and thrombin concentrations promote neuronal rather than glial growth when primary neural cells are seeded within plasma-derived fibrin gels. Tissue Eng Part A 2010;16(5): 1607–1619; doi: 10.1089/TEN.TEA.2009.0372
- Engler AJ, Griffin MA, Sen S, et al. Myotubes differentiate optimally on substrates with tissue-like stiffness: Pathological implications for soft or stiff microenvironments. J Cell Biol 2004;166(6):877; doi: 10.1083/JCB.200405004
- 23. Poisson JS, Acker JP, Briard JG, et al. Modulating intracellular ice growth with cell-permeating small-molecule ice recrystallization inhibitors. Langmuir 2019;35(23):7452–7458; doi: 10.1021/acs.langmuir.8b02126
- Chang T, Zhao G. Ice Inhibition for cryopreservation: Materials, strategies, and challenges. Adv Sci 2021;8(6): 2002425; doi: 10.1002/ADVS.202002425
- 25. McGann LE, Walterson ML. Cryoprotection by dimethyl sulfoxide and dimethyl sulfone. Cryobiology 1987;24(1): 11–16; doi: 10.1016/0011-2240(87)90003-4
- 26. Jiang S, Lyu C, Zhao P, et al. Cryoprotectant enables structural control of porous scaffolds for exploration of cellular mechano-responsiveness in 3D. Nat Commun 2019;10(1):3491; doi: 10.1038/S41467-019-11397-1
- Murphy CM, Haugh MG, O'Brien FJ. The effect of mean pore size on cell attachment, proliferation and migration in collagen–glycosaminoglycan scaffolds for bone tissue engineering. Biomaterials 2010;31(3):461–466; doi: 10.1016/ J.BIOMATERIALS.2009.09.063
- 28. Rouwkema J, Koopman BFJM, Blitterswijk CAV, et al. Supply of nutrients to cells in engineered tissues. Biotechnol Genet Eng Rev 2010;26(1):163–178; doi: 10.5661/BGER-26-163
- 29. Lien SM, Ko LY, Huang TJ. Effect of pore size on ECM secretion and cell growth in gelatin scaffold for articular cartilage tissue engineering. Acta Biomater 2009;5(2):670–679; doi: 10.1016/j.actbio.2008.09.020
- 30. Kim T, Ahmad K, Shaikh S, et al. Dermatopontin in skeletal muscle extracellular matrix regulates myogenesis. Cells 2019;8(4):332; doi: 10.3390/CELLS8040332
- Zhang W, Liu Y, Zhang H. Extracellular matrix: An important regulator of cell functions and skeletal muscle development. Cell Biosci 2021;11(1):1–13; doi: 10.1186/S13578-021-00579-4
- 32. Liu X, Gao Y, Long X, et al. Type I collagen promotes the migration and myogenic differentiation of C2C12 myoblasts via the release of interleukin-6 mediated by FAK/ NF-κB p65 activation. Food Funct 2020;11(1):328–338; doi: 10.1039/C9FO01346F

 Chen X, Li Y. Role of matrix metalloproteinases in skeletal muscle: Migration, differentiation, regeneration and fibrosis. Cell Adh Migr 2009;3(4):337; doi: 10.4161/CAM.3.4.9338

- 34. Ascenzi F, Barberi L, Dobrowolny G, et al. Effects of IGF-1 isoforms on muscle growth and sarcopenia. Aging Cell 2019;18(3):e12954; doi: 10.1111/ACEL.12954
- 35. Schiaffino S, Mammucari C. Regulation of skeletal muscle growth by the IGF1-Akt/PKB pathway: Insights from genetic models. Skelet Muscle 2011;1(1):1–14; doi: 10.1186/2044-5040-1-4/FIGURES/4
- 36. Barua B, Winkelmann DA, White HD, et al. Regulation of actin-myosin interaction by conserved periodic sites of tropomyosin. Proc Natl Acad Sci U S A 2012;109(45): 18425–18430; doi: 10.1073/PNAS.1212754109

Address correspondence to:
Rashid Bashir, PhD
Department of Bioengineering
University of Illinois at Urbana-Champaign
306 Engineering Hall, MC-266
1308 Wright Green Street
Urbana, IL 61801
USA

E-mail: rbashir@illinois.edu

Received: April 11, 2023 Accepted: July 14, 2023

Online Publication Date: August 11, 2023